COMPARISON OF THREE TECHNIQUES FOR SOLVING THE RADIATIVE TRANSPORT EQUATION

J. A. Roux and A. M. Smith
ARO, Inc.

VON KÁRMÁN GAS DYNAMICS FACILITY
ARNOLD ENGINEERING DEVELOPMENT CENTER
AIR FORCE SYSTEMS COMMAND
ARNOLD AIR FORCE STATION, TENNESSEE 37389

January 1974

Final Report for Period 1 August 1972 — 31 July 1973

Approved for public release; distribution unlimited.

Prepared for

ARNOLD ENGINEERING DEVELOPMENT CENTER (XON)
ARNOLD AIR FORCE STATION, TENNESSEE 37389

NOTICES

When U. S. Government drawings specifications, or other data are used for any purpose other than a definitely related Government procurement operation, the Government thereby incurs no responsibility nor any obligation whatsoever, and the fact that the Government may have formulated, furnished, or in any way supplied the said drawings, specifications, or other data, is not to be regarded by implication or otherwise, or in any manner licensing the holder or any other person or corporation, or conveying any rights or permission to manufacture, use, or sell any patented invention that may in any way be related thereto.

Qualified users may obtain copies of this report from the Defense Documentation Center.

References to named commercial products in this report are not to be considered in any sense as an endorsement of the product by the United States Air Force or the Government.

APPROVAL STATEMENT

This technical report has been reviewed and is approved.

Melvin L. Guiou

MELVIN L. GUIOU
Captain, USAF
Research and Development
Division
Directorate of Technology

Robert O Dietz

ROBERT O. DIETZ
Director of Technology

UNCLASSIFIED

SECURITY CLASSIFICATION OF THIS PAGE *(When Data Entered)*

REPORT DOCUMENTATION PAGE		READ INSTRUCTIONS BEFORE COMPLETING FORM
1 REPORT NUMBER AEDC-TR-73-200	2 GOVT ACCESSION NO.	3 RECIPIENT'S CATALOG NUMBER
4 TITLE *(and Subtitle)* COMPARISON OF THREE TECHNIQUES FOR SOLVING THE RADIATIVE TRANSPORT EQUATION		5 TYPE OF REPORT & PERIOD COVERED Final Report - 1 August 1972 to 31 July 1973 6. PERFORMING ORG REPORT NUMBER
7. AUTHOR(s) J. A. Roux and A. M. Smith, ARO, Inc.		8. CONTRACT OR GRANT NUMBER(s)
9 PERFORMING ORGANIZATION NAME AND ADDRESS Arnold Engineering Development Center Arnold Air Force Station, Tennessee 37389		10 PROGRAM ELEMENT, PROJECT, TASK AREA & WORK UNIT NUMBERS 65802F
11 CONTROLLING OFFICE NAME AND ADDRESS Arnold Engineering Development Center (XON) Arnold Air Force Station, Tennessee 37389		12 REPORT DATE January 1974 13. NUMBER OF PAGES 39
14. MONITORING AGENCY NAME & ADDRESS *(If different from Controlling Office)*		15. SECURITY CLASS *(of this report)* UNCLASSIFIED 15a. DECLASSIFICATION/DOWNGRADING SCHEDULE N/A

16 DISTRIBUTION STATEMENT *(of this Report)*

Approved for public release; distribution unlimited.

17. DISTRIBUTION STATEMENT *(of the abstract entered in Block 20, if different from Report)*

18. SUPPLEMENTARY NOTES

Available in DDC.

19 KEY WORDS *(Continue on reverse side if necessary and identify by block number)*

cryogenic temperature	cryopumping
radiation	monochromatic radiation
heat transfer	reflectance

20 ABSTRACT *(Continue on reverse side if necessary and identify by block number)*

The source function formulation of the radiative transport equation is solved by successive approximations; the discrete ordinate formulation is solved by both the Milne predictor-corrector and Chandrasekhar techniques. These three techniques are compared with respect to applicability and computation time, and a brief error analysis is given for each. A comparison is shown between the double and single Gaussian quadratures (orders

DD FORM 1 JAN 73 1473 EDITION OF 1 NOV 65 IS OBSOLETE

UNCLASSIFIED

SECURITY CLASSIFICATION OF THIS PAGE *(When Data Entered)*

20, Continued

10 through 96) used in the discrete ordinate formulation. The effect of refractive index on the quadrature order necessary to obtain accuracy for Fresnel boundaries is shown.

PREFACE

The work reported herein was conducted by the Arnold Engineering Development Center (AEDC), Air Force Systems Command (AFSC). The work was done by ARO, Inc. (a subsidiary of Sverdrup & Parcel and Associates, Inc.), contract operator of AEDC, AFSC, Arnold Air Force Station, Tennessee. The work was performed under ARO Project No. VF215, and the manuscript (ARO Control No. ARO-VKF-TR-73-137) was submitted for publication on October 1, 1973.

CONTENTS

ILLUSTRATIONS

TABLES

1.0 INTRODUCTION

The formation of condensed gases on cryogenically cooled surfaces has recently received attention in regard to how the resulting coating affects the reflection and transmission of visible and infra-red (IR) radiation. Sensor testing requires knowledge of condensed gas coating reflectances and transmittances because film deposits formed on the sensor system transfer optics (which are cryogenically cooled) can affect their absolute throughput. These condensed gas deposits both absorb and scatter visible and IR radiation. Scattering and absorption are functions of both wavelength and coating thickness. In addition, if collimated light is incident upon optical surfaces coated with condensed gases, the transmitted and reflected light will no longer be collimated. Thus it becomes important to know the angular distribution of the reflected and transmitted energy. Presently, work is under way to experimentally determine the effects of gas deposits formed on cryogenically cooled (20°K) lenses, filters, windows, mirrors, and opaque substrates such as black paint and stainless steel.

Experimental data are important in determining the effects of coating thickness and viewing angle, as well as wavelength, upon reflectance and transmittance. However, it is useful to have analytical or theoretical expressions which mathematically model the reflectance and transmittance behavior. First, the analytical expressions are valuable in understanding the reasons behind the behavior of the experimental data. (Also, the theoretical expressions can be used to determine the magnitude of the various contributing processes such as scattering, absorption, substrate effects, front interface reflectance, etc. In this regard, the theory really complements the experimental data.) Second, when the theory and the data both show the same quantitative behavior (as in Ref. 1), then the theory and experimental data may be used to determine the thickness and important optical properties of the condensed gas coating such as refractive index, absorption index, scattering coefficient, and absorption coefficient. When scattering and absorption are both present, the optical properties and thickness may be obtained through using experimental data in conjunction with the solution to the radiative transport equation (as was done in Ref. 1).

The results obtained in Ref. 1 were determined by solving the radiative transport equation by the Milne predictor-corrector method. This method works, but it is cumbersome to use and requires a significant amount of computer time. In an attempt to find a simpler and

faster technique, three different methods for solving the radiative transport equation are presented and compared. First, the transport equation is solved iteratively by the Milne predictor-corrector finite-difference method. Second, an integral equation formulation for the source function is solved by successive approximations; knowing the source function leads directly to obtaining the intensity as a function of viewing angle and optical thickness. Third, the Chandrasekhar eigenvalue, eigenvector solution is shown in comparison with the other two techniques. It is important to have several solution techniques because each technique possesses a distinct advantage over the others. The Chandrasekhar method is simple and fast, but it is applicable only when the absorption and scattering coefficients are not functions of coating thickness. The other two techniques are still applicable even when the optical properties vary with coating thickness.

In choosing three techniques for comparison, it is useful to review some previous work requiring solution of the radiative transport equation. Wolf (Ref. 2) numerically solved the transformed (by discrete ordinates) transport equation via Simpson's rule. After reducing the transport equation to a system of linear ordinary differential equations, Wolf obtained solutions for problems involving absorbing, emitting, and scattering media with an arbitrary specified temperature profile. In Ref. 1 the Milne predictor-corrector numerical scheme was used to investigate the reflectance behavior of absorbing and internally scattering cryodeposits.

The formulation of an expression for the source function was performed by Merriam (Ref. 3). Merriam's technique leads to an integral equation, the solution of which describes the source function. Once the source function is known, the radiant intensity behavior can be directly computed.

Besides the integral equation formulation and the numerical solution, other solutions to the transport equation have been obtained through the computation of eigenvalues and eigenvectors. When a Gaussian quadrature (discrete ordinates) is used to approximate the integral term in the transport equation, a system of simultaneous differential equations is obtained. The eigenvalues and eigenvectors associated with the coefficient matrix of the system of differential equations can be used to obtain the homogeneous solutions; emission gives rise to particular solutions. Once the general solution is known, the boundary conditions are enforced to evaluate the integration constants. Hottel, et al. (Ref. 4) employed the method of discrete coordinates to compute the biangular

reflectance from an absorbing and anisotropically scattering medium. The system of differential equations was solved by computing the eigenvalues and eigenvectors. Merriam (Ref. 3) has also made use of the method of discrete ordinates; eigenvalues and eigenvectors were computed by the "method of Danilevsky" as described by Faddeeva (Ref. 5). Hsia and Love (Ref. 6) also have published a computational method of monochromatic heat transfer in the plane, one-dimensional case of a parallel atmosphere separated by a cloud of particles. Applying the method of discrete ordinates, they solved the resulting set of differential equations by obtaining eigenvalues and eigenvectors utilizing the method of idempotents. Another particularly attractive method for the computation of eigenvalues and eigenvectors for solution of the transport equation in association with both isotropic and anisotropic scattering is that of Chandrasekhar (Ref. 7). Chandrasekhar's method yields an equation which readily permits the extraction of the eigenvalues instead of requiring, as in Ref. 5, the determination of the characteristic polynominal before attempting computation of the eigenvalues. In addition to the works mentioned above there are numerous other solution methods such as considering radiant transport through optically thick media to be a diffusion process (Ref. 8). Also, the transport equation has been solved by Callis via the method of characteristics (Ref. 9).

As mentioned earlier, the three techniques chosen for study are the Chandrasekhar method, the source function integral equation formulation, and a numerical solution by the Milne predictor-corrector scheme. These three were chosen because they are easy to understand and simple to apply, and because they serve as useful tools to the engineer. Also, it is useful to have several different solution techniques available, as one technique may possess a distinct advantage over the others. In order to form a basis for comparison of the three solution techniques, a standard problem has been selected to which the different methods will be applied. The problem chosen is that of an absorbing and isotropically scattering dielectric medium which will be more fully described in the next section of this report. Isotropic scattering was assumed in order to avoid perplexion with a highly sophisticated scattering function. However, all three methods presented can be extended for application to anisotropically scattering media. Emission was considered negligible in order not to require particular solutions nor to have to choose a specific temperature profile or temperature level. Again, the three techniques discussed here can easily be extended to include emission once the temperature profile and level of temperature have been prescribed.

The three solution procedures are compared with one another, and the Chandrasekhar method is used to make a comparison between results obtained by single and double Gaussian quadratures. Hottel, et al. (Ref. 4) have used both double and single Gaussian quadrature approximations in response to the proposal in Ref. 10 that, because of the discontinuity of the intensity for $\mu = 0$ at the bounding interfaces, the quadrature formulas should be applied separately in the μ ranges of -1 to 0 and 0 to 1. They employed as many as 20 double Gaussian quadrature directions (points) and 24 single Gaussian quadrature directions and observed no appreciable difference between the two types of quadratures. Hsia and Love (Ref. 6) have used the double Gaussian quadrature (8 points) in their work, whereas Wolf (Ref. 2, 8 points), Roux (Ref. 1, 10 points), Merriam (Ref. 3, 24 points), and Chandrasekhar (Ref. 7) have all employed the single Gaussian quadrature. One purpose of this paper is to determine whether there is any computational advantage (with respect to accuracy, convenience, or computer time) of using the single as compared to the double Gaussian quadrature. In addition, for each quadrature approximation the influence of the number of quadrature points is investigated; as many as 96 points were used for the single Gaussian quadrature, and as many as 48 points were utilized for the double Gaussian quadrature.

2.0 STATEMENT OF THE PROBLEM

In order to compare the three techniques for solving the transport equation it was necessary to select a sample problem to which they would be applied. The geometry and coordinate system for the selected problem are shown in Fig. 1. The nomenclature employed in Fig. 1 is essentially the same as that used in Refs. 1 and 3; regions 1, 2, and 3 respectively represent vacuum, radiatively participating medium, and opaque substrate. The radiant intensity (I_o) incident on the radiatively participating (dielectric) medium from vacuum is taken to be diffusely distributed. The dielectric coating is partially transparent, and the opaque substrate is considered to be either a conductor or a dielectric having negligible emission. The vacuum-coating interface is assumed to reflect radiant intensity in accordance with Fresnel's equations and to transmit radiant intensity according to Snell's law. The substrate is taken to be a Fresnel reflector. Since the interface reflectance for radiant intensity traveling from vacuum to coating and the interface reflectance for intensity traversing from coating to vacuum are not the same for equal angles of incidence, the two interface reflectances

are designated as ρ_{12} and ρ_{21}, respectively. Also, the interface reflectance for intensity incident on the substrate is designated as ρ_{23}. Further, the interior of the radiatively participating coating is considered to be absorbing and isotropically scattering with negligible emission. Furthermore, the absorption and scattering coefficients (and hence albedo) are considered not to be functions of the local position y in the participating film. In addition, the radiative intensity is assumed to be axisymmetric; this means that the intensity field is dependent on the polar angle θ but not on the aximuthal angle ϕ. The sample problem thus defined via Fig. 1 was used to compare the three solution procedures through the prediction by each technique of the monochromatic hemispherical-directional reflectance.

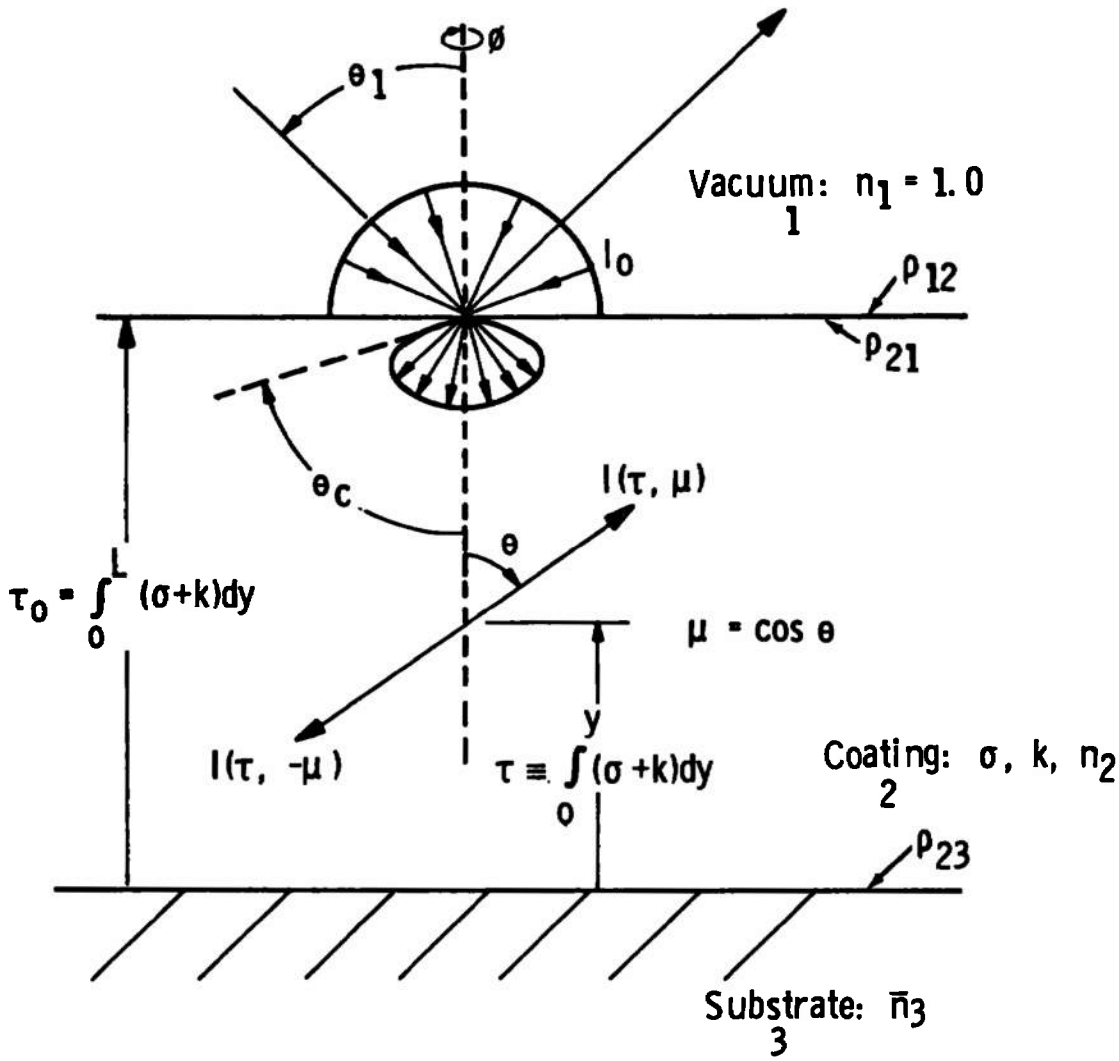

Figure 1. Coordinate system and geometry.

3.0 ANALYSIS

Now that the sample problem has been physically defined, the mathematical presentation of the governing equations will be given. After the transport equation and boundary conditions are shown, each of the three solution techniques will be applied to the problem as a subsection of the analysis. The radiative transport equation subject to the above stated assumptions is

$$\frac{di(\tau,\mu)}{d\tau} = \frac{-i(\tau,\mu)}{\mu} + \frac{W}{2\mu}\int_{-1}^{1} i(\tau,\mu')d\mu' \tag{1}$$

where $i(\tau,\mu)$ is the local radiant intensity, $I(\tau,\mu)$, nondimensionalized by the diffusely incident intensity I_o (Fig. 1); μ is the cosine of the internal polar angle θ defining the direction of $I(\tau,\mu)$; $W = \sigma/(\sigma+k)$ is the albedo parameter; and τ is the local optical depth, which is related to the position coordinate y by

$$\tau = \int_{o}^{y}(\sigma + k)dy \tag{2}$$

with σ and k being the scattering and absorption coefficients, respectively. As previously stated, the coating boundaries were considered to have only regular Fresnel reflection and refraction; expressed mathematically, these boundary conditions are

$$i(\tau_o,-\mu) = \rho_{21}(\mu)\, i(\tau_o,\mu) - \left[1 - \rho_{12}(\mu^1)\right]n_2^2 \tag{3}$$

for the vacuum-coating interface and

$$i(0,\mu) = \rho_{23}(\mu)\, i(0,-\mu) \tag{4}$$

for the coating-substrate interface where n_2 is the refractive index of the coating and μ^1 is the cos θ_1, with θ_1 being the polar angle external to the radiatively participating medium (Fig. 1). The directions μ and μ^1 are related by Snell's law,

$$\mu^1 = \left[1 - \left(1 - \mu^2\right)n_2^2\right]^{1/2} \tag{5}$$

and $\tau_o = \tau(y=L)$ where L is the coating geometrical thickness.

3.1 METHOD OF CHANDRASEKHAR

The basic objective of the method of Chandrasekhar is computation of the eigenvalues and eigenvectors of the coefficient matrix associated

with the system of simultaneous ordinary linear differential equations resulting from the use of discrete ordinates. Once the eigenvalues and eigenvectors are determined, the homogeneous solution is known; the integration constants are then directly obtainable from the boundary conditions. Before the eigenvalues and eigenvectors can be computed, the transport equation, Eq. (1), together with the boundary conditions, Eqs. (3) and (4), must be first transformed into a system of differential equations by the method of discrete ordinates. This consists of replacing the integral term in Eq. (1) by a Gaussian quadrature of the form

$$\int_{-1}^{1} f(x)dx = \sum_{j=1}^{r} a_j f(x_j) \tag{6}$$

where x_j is the quadrature points (discrete ordinates), a_j is the quadrature weights, and p (which is an even integer) is the order of the quadrature approximation. Replacing the integral term in Eq. (1) by Eq. (6) yields a system of p simultaneous differential equations

$$\frac{di(\tau,\mu_\ell)}{d\tau} = \frac{-i(\tau,\mu_\ell)}{\mu_\ell} + \frac{W}{2\mu_\ell}\sum_{j=1}^{p} a_j i(\tau,\mu_j), \quad \ell=1,\ldots,p \tag{7}$$

with boundary conditions

$$i(\tau_o,-\mu_\ell) = \rho_{21}(\mu_\ell)i(\tau_o,\mu_\ell) + \left[1-\rho_{12}\left(\mu_\ell^1\right)\right]n_2^2, \quad \ell=1,\ldots,p/2 \tag{8}$$

and

$$i(0,\mu_\ell) = \rho_{23}(\mu_\ell)i(0,-\mu_\ell) \quad , \quad \ell=1,\ldots,p/2 \tag{9}$$

The coefficient matrix of Eq. (7) can be written as

$$B_{\ell j} = (Wa_j/2-\delta_{\ell j})/\mu_\ell \quad , \quad \ell,j = 1,\ldots,p \tag{10}$$

where $\delta_{\ell j}$ is the Kronecker delta. This matrix has exactly the same form whether the single Gaussian quadrature is employed over the interval $-1 \leq \mu \leq 1$ as shown in Eq. (6) or whether the double Gaussian quadrature is used separately in the regions 0 to 1 and -1 to 0. For the latter case, the double Gaussian quadrature of order p/2 is used twice, thus giving a p x p coefficient matrix of the form in Eq. (10). The quadrature points and weights are different for the two cases, but in both instances they possess the common properties

$$\mu_k = -\mu_{p+1-k} \quad , \quad a_k = a_{p+1-k} \quad , \quad k = 1,\ldots,p/2 \tag{11}$$

It has been shown (Ref. 11) that the p eigenvalues associated with the p x p coefficient matrix, Eq. (10), are the p values of λ which satisfy the expression

$$\left[\prod_{j=1}^{p/2}(1-\mu_j^2\lambda^2)\right]\left[W\sum_{j=1}^{p/2}\frac{a_j\mu_j^2\lambda^2}{1-\mu_j^2\lambda^2}-(1-W)\right]=0 \qquad (12)$$

Note that Eq. (12) is a function of λ^2. It is known that the roots λ^2 are positive or zero as shown in Fig. 2. Thus, the eigenvalues occur as plus and minus pairs. When W = 0, the first factor of Eq. (12) must be zero, giving the p eigenvalues as $\lambda_j = \pm 1/\mu_j$, j = 1, . . . , p/2. If

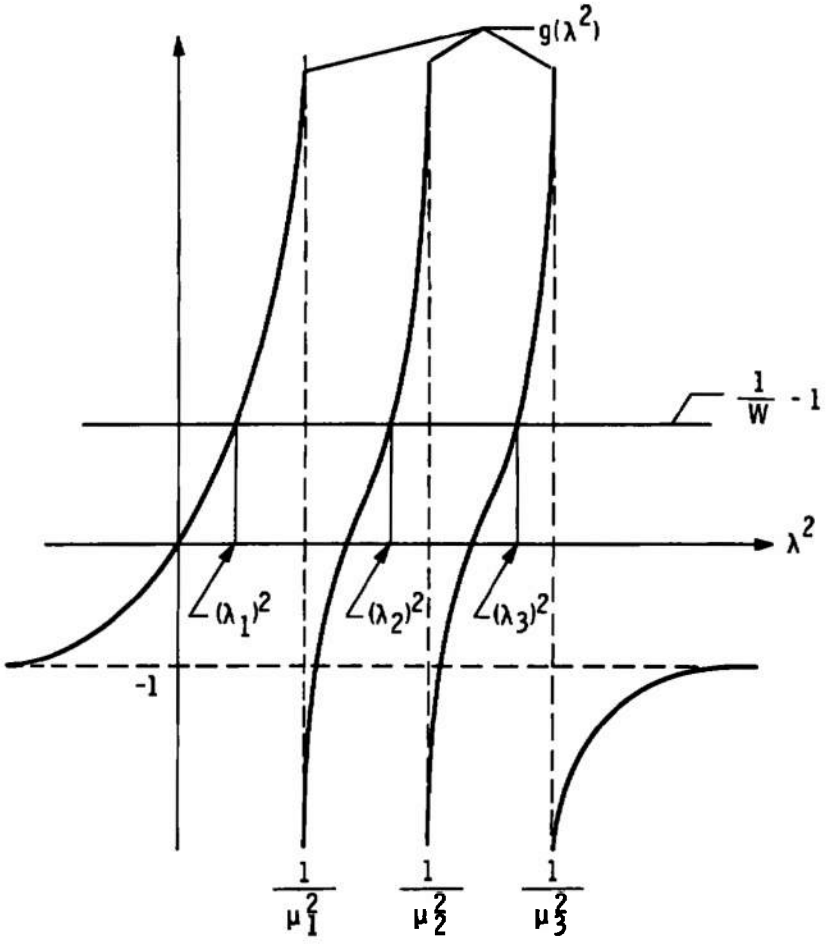

Note: Plot is not to scale.

Figure 2. Sketch illustrating graphical solution for the eigenvalues, p = 6, Ref. 11.

$W \neq 0$, the second factor must be zero. Setting the second factor equal to zero and simplifying, one finds the eigenvalues must satisfy the equation

$$g(\lambda^2) = \sum_{j=1}^{p/2} \frac{a_j \mu_j^2 \lambda^2}{\left(1 - \mu_j^2 \lambda^2\right)} = \frac{1}{W} - 1 \tag{13}$$

which is equivalent to that obtained in Ref. 7,

$$\sum_{j=1}^{p/2} \frac{a_j}{1 - \lambda^2 \mu_j^2} = \frac{1}{W} \tag{14}$$

if one notes that the term -1 on the right side of Eq. (13) is equivalent to $-\sum_{j=1}^{p/2} a_j$. When $W = 1.0$, the right side of Eq. (13) is zero, and it is seen that $\lambda^2 = 0$ is a root. Thus, zero is an eigenvalue with multiplicity of two and requires a special form of the homogeneous solution in order to insure linearly independent solutions. Plotting simultaneously $g(\lambda^2)$ and $1/W-1$ versus λ^2 yields the solutions λ^2 where $g(\lambda^2)$ and $(1/W-1)$ intersect. Figure 2 is an illustrative plot for $p = 6$, but the analysis is valid for any even integer p. It is seen from Fig. 2 that the values λ^2 satisfying Eq. (13) must be positive or zero. Thus, all the eigenvalues must be real and must occur in plus and minus pairs except for $W = 1$, where two of the eigenvalues are equal to zero. Also, from Fig. 2 one can readily establish the bounds for the roots λ^2. For this example, $0 \leq \lambda_1^2 \leq 1/\mu_1^2 < \lambda_2^2 \leq 1/\mu_2^2 < \lambda_3^2 \leq 1/\mu_3^2$. Thus all the roots λ^2 have individual bounds. Using these bounds, the numerical solution for the roots of Eq. (13) may be easily obtained. The homogeneous solution of Eq. (7) for $W \neq 1.0$ is given by

$$i(r,\mu_\ell) = \sum_{j=1}^{p/2} \frac{1 - \lambda_j \mu_j}{1 - \lambda_j^2 \mu_\ell^2} \left[c_j (1 - \lambda_j \mu_\ell) e^{\lambda_j r} - c_{p+1-j} (1 + \lambda_j \mu_\ell) e^{-\lambda_j r} \right] , \quad \ell = 1,\ldots,p \tag{15}$$

where the c's are the p number of integration constants determined from the boundary conditions. Substitution of Eq. (15) into Eqs. (8) and (9) yields a system of p nonhomogeneous linear algebraic equations to be solved for the p values of c; use of the Gauss-Jordon method or Cholesky method (see Ref. 12) readily allows determination of the integration constants. For the special case of $W = 1.0$, the double eigenvalue $\lambda_1 = \lambda_p = 0$ causes Eq. (15) to have the special form (Ref. 13)

$$i(r,\mu_\ell) = c_1 + c_p (r - \mu_\ell) + \sum_{j=2}^{p/2} \frac{1 - \lambda_j \mu_j}{1 - \lambda_j^2 \mu_\ell^2} \left[c_j (1 - \lambda_j \mu_\ell) e^{-\lambda_j r} - c_{p+1-j} (1 + \lambda_j \mu_\ell) e^{-\lambda_j r} \right] , \quad \ell = 1,\ldots,p \tag{16}$$

Chandrasekhar (Ref. 7) also has expressions equivalent to Eqs. (15) and (16) if one defines the Chandrasekhar integration constants, c_j^1 and c_{p+1-j}^1, as

$$c_j^1 = (1 - \lambda_j \mu_j) c_j \quad \text{and} \quad c_{p+1-j}^1 = (1 - \lambda_j \mu_j) c_{p+1-j} \tag{17}$$

It should be noted that Eqs. (15) and (16) yield the solution of Eq. (7) in the p quadrature directions. If information is required in directions other than the quadrature directions, then interpolation must be used among the solutions in the quadrature directions. A final comment stressing the simplicity of this technique is that once the eigenvalues are obtained from Eq. (13) (which is easily done since their bounds are known), the homogeneous solution is immediately given by Eq. (15) or, if W = 1.0, by Eq. (16). Only the integration constants remain to be found, and these can readily be obtained by standard computer library routines for solving systems of nonhomogeneous linear algebraic equations.

The eigenvectors have already been included in Eqs. (15) and (16), and they are functions only of the quadrature points and the eigenvalues. Information on the derivation of the eigenvectors is available in Refs. 7, 11, and 13.

3.2 SOURCE FUNCTION FORMULATION

Solution of the transport equation, Eq. (1), along with the boundary conditions, Eqs. (3) and (4), through the source function formulation was accomplished by solving an integral equation describing the source function. The intensity field was then computed through its direct relation to the source function. In order to arrive at the integral equation, let Eq. (1) be rewritten as

$$\frac{di(\tau,\mu)}{d\tau} - \frac{i(\tau,\mu)}{\mu} = \frac{\Phi(\tau)}{\mu} \tag{18}$$

where $\Phi(\tau)$ is the normalized source function

$$\Phi(\tau) = \frac{W}{2}\left[\int_0^1 i(\tau,-\mu')d\mu' - \int_0^1 i(\tau,\mu')d\mu'\right] \tag{19}$$

Solving Eq. (18) for the normalized intensity yields solutions for the intensity in the upward (positive μ) and downward (negative μ) directions as

$$i(\tau,\mu) = i(0,\mu)e^{-\tau/\mu} + \int_0^{\tau} \Phi(t)e^{-(\tau-t)/\mu} \frac{dt}{\mu} \tag{20}$$

and

$$i(\tau,-\mu) = i(\tau_o,-\mu)e^{-(\tau_o-\tau)/\mu} + \int_{\tau}^{\tau_o} \Phi(t)e^{-(t-\tau)/\mu} \frac{dt}{\mu} \tag{21}$$

where now in Eqs. (20) and (21) $0 \leq \mu \leq 1.0$. From Eqs. (20) and (21) it is observed that the intensity in the upward and downward directions is directly related to the normalized source function. Hence, once the source function is known, the intensity field can be directly evaluated. The procedure to be followed here in determining the source function is first to find $i(0,\mu)$ and $i(\tau_o, -\mu)$ in Eqs. (20) and (21) through the boundary conditions. Once $i(0,\mu)$ and $i(\tau_o, -\mu)$ are known, then Eqs. (20) and (21) are substituted into Eq. (19), resulting in one integral equation to be solved for the one unknown, $\Phi(\tau)$.

For the problem defined in this paper, the integral equation is obtained by proceeding as outlined above. From Eqs. (20) and (21) it is found that

$$i(\tau_o,\mu) = i(0,\mu)e^{-\tau_o/\mu} + \int_0^{\tau_o} \Phi(t)e^{-(\tau_o-t)/\mu} \frac{dt}{\mu} \tag{22}$$

and

$$i(0,-\mu) = i(\tau_o,-\mu)e^{-\tau_o/\mu} + \int_0^{\tau_o} \Phi(t)e^{-t/\mu} \frac{dt}{\mu} \tag{23}$$

Substituting the expressions $i(\tau_o,\mu)$ and $i(0, -\mu)$ from Eqs. (22) and (23) into Eqs. (3) and (4) readily yields the values $i(0,\mu)$ and $i(\tau_o, -\mu)$ needed in Eqs. (20) and (21). With $i(0,\mu)$ and $i(\tau_o, -\mu)$ known, Eqs. (20) and (21) are substituted into Eq. (19), which, after the indicated algebra is performed, becomes the integral equation describing $\Phi(\tau)$,

$$\Phi(\tau) = \frac{W}{2}\left[\int_0^1 \frac{[1-\rho_{12}(\mu^1)]n_2^2\,\rho_{23}(\mu)e^{-(\tau_o-\tau)/\mu}}{D(\tau_o,\mu)}\,d\mu + \int_0^1 \frac{[1-\rho_{12}(\mu^1)]n_2^2\,e^{-(\tau_o-\tau)/\mu}}{D(\tau_o,\mu)}\,d\mu\right.$$

$$+ \int_0^{\tau_o}\Phi(t)\int_0^1 e^{-(|\tau-t|)/\mu}\,\frac{d\mu}{\mu}\,dt + \int_0^{\tau_o}\Phi(t)\int_0^1 \frac{\rho_{23}(\mu)e^{-(\tau_o+t)/\mu}}{D(\tau_o,\mu)}\,\frac{d\mu}{\mu}\,dt$$

$$+ \int_0^{\tau_o}\Phi(t)\int_0^1 \frac{\rho_{23}(\mu)\,\rho_{21}(\mu)e^{-(2\tau_o+\tau-t)/\mu}}{D(\tau_o,\mu)}\,\frac{d\mu}{\mu}\,dt + \int_0^{\tau_o}\Phi(t)\int_0^1 \frac{\rho_{21}(\mu)e^{-(2\tau_o-\tau-t)/\mu}}{D(\tau_o,\mu)}\,\frac{d\mu}{\mu}\,dt$$

$$\left. + \int_0^{\tau_o}\Phi(t)\int_0^1 \frac{\rho_{23}(\mu)\,\rho_{21}(\mu)e^{-(2\tau_o-\tau+t)/\mu}}{D(\tau_o,\mu)}\,\frac{d\mu}{\mu}\,dt\right] \qquad (24)$$

where

$$D(\tau_o,\mu) = 1-\rho_{21}(\mu)\,\rho_{23}(\mu)e^{-2\tau_o/\mu} \qquad (25)$$

The solution of Eq. (24) was obtained through the method of successive approximations. At first glance Eq. (24) appears to be quite complicated; however, closer observation reveals that this is not so. First notice that the integrands of the first two integrals of Eq. (24) are all known functions, hence these integrals only need to be evaluated once. Since their values can readily be computed, these terms do not have to be reevaluated during the process of successive approximations. A similar observation is noticeable concerning the integration with respect to μ in the last five terms on the right side of Eq. (24). In the last five terms of Eq. (24) all the functions which are integrated with respect to μ are known functions; thus the integration with respect to μ need only be performed once during the process of successive approximations. These observations can result in a significant saving of computer time, but a large amount of storage is required since the values of the integrals with respect to μ in the last five terms of Eq. (24) must be stored at each t and τ combination (t occurs in the exponent of the exponential inside the integration with respect to μ).

The solution of Eq. (24) was determined at discrete τ values by the method of successive approximations. The integration with respect to μ was performed by using 10 Gaussian quadrature points. The

integration with respect to t was accomplished via Simpson's rule with the optical thickness, τ_o, divided into 50 equal intervals. The initial guess at the solution for $\Phi(\tau)$ was $\Phi(\tau) = 0.0$. The initial guess at $\Phi(\tau)$ is substituted into the right-hand side of Eq. (24), and an improved estimate of $\Phi(\tau)$ is computed. This process is repeated until convergence is considered to have been obtained. In this work the successive approximations were repeated until the maximum difference between two successive calculations of $\Phi(\tau)$ at any τ station was less than 0.0001. Once the process of successive approximations has converged, the value $i(\tau_o, \mu)$ can be directly computed from

$$i(\tau_o,\mu) = \left\{\left[1 - \rho_{12}(\mu^1)\right]n_2^2 \rho_{23}(\mu)e^{-2\tau_o/\mu} + \int_o^{\tau_o} \Phi(t)e^{-(\tau_o - t)/\mu} \frac{dt}{\mu}\right.$$

$$\left. + \rho_{23}(\mu) \int_o^{\tau_o} \Phi(t)e^{-(\tau_o + t)/\mu} \frac{dt}{\mu}\right\} \Big/ \left\{1 - \rho_{21}(\mu)\rho_{23}(\mu)e^{-2\tau_o/\mu}\right\} \qquad (26)$$

The integrals in Eq. (26) were again evaluated via Simpson's rule. The expression $i(\tau_o, \mu)$, as will be shown, is needed to compute the hemispherical-directional reflectance. Note that Eq. (26) yields information in the quadrature directions and in all other directions; no interpolation is required to obtain information in the nonquadrature directions, as is necessary for the Chandrasekhar method and the predictor-corrector numerical solution.

3.3 NUMERICAL SOLUTION

After the transport equation and boundary conditions, Eqs. (1), (3), and (4), were transformed by the use of discrete ordinates into the system of equations given in Eqs. (7) through (9), solution was obtained by the Milne predictor-corrector method. The system of equations to be solved is the same system as that solved by the Chandrasekhar method. The primary advantage of the numerical solution (and source function formulation) is that the system of differential equations can be allowed to have variable coefficients; the Chandrasekhar method, although powerful, is applicable only when the system of differential equations has constant coefficients. In the application of the predictor-corrector method to the system of equations, the number of steps utilized in the numerical calculations was varied from 50 to 200. The mathematical expressions for the predictor-corrector method adapted to $i(\tau, \mu_\ell)$, $\ell = 1, \ldots, p/2$ are

Predictor

$$i(\tau_{n+1},\mu_\ell) = i(\tau_{n-3},\mu_\ell) + \frac{4h}{3}\left[2\frac{di}{d\tau}(\tau_n,\mu_\ell) - \frac{di}{d\tau}(\tau_{n-1},\mu_\ell) + 2\frac{di}{d\tau}(\tau_{n-2},\mu_\ell)\right] \quad (27)$$

Corrector

$$i(\tau_{n+1},\mu_\ell) = i(\tau_{n-1},\mu_\ell) + \frac{h}{3}\left[\frac{di}{d\tau}(\tau_{n-1},\mu_\ell) + 4\frac{di}{d\tau}(\tau_n,\mu_\ell) + \frac{di}{d\tau}(\tau_{n+1},\mu_\ell)\right] \quad (28)$$

and for $i(\tau,\mu_\ell)$, $\ell = p/2 + 1, \ldots, p$ are

Predictor

$$i(\tau_{m-1},\mu_\ell) = i(\tau_{m+3},\mu_\ell) + \frac{4h}{3}\left[2\frac{di}{d\tau}(\tau_m,\mu_\ell) - \frac{di}{d\tau}(\tau_{m+1},\mu_\ell) + 2\frac{di}{d\tau}(\tau_{m+2},\mu_\ell)\right] \quad (29)$$

Corrector

$$i(\tau_{m-1},\mu_\ell) = i(\tau_{m+1},\mu_\ell) + \frac{h}{3}\left[\frac{di}{d\tau}(\tau_{m+1},\mu_\ell) + 4\frac{di}{d\tau}(\tau_m,\mu_\ell) + \frac{di}{d\tau}(\tau_{m-1},\mu_\ell)\right] \quad (30)$$

where $n = 4, 5, \ldots, N$ and $m = N-4, N-3, \ldots 1$ with N being the number of stations employed in marching from 0 to τ_o, and h the step size, $h = \tau_o/(N-1)$.

In order to use Eq. (27), one must know the derivatives at τ_n, τ_{n-1}, and τ_{n-2}. These values can be determined directly from the differential equations only after the corresponding values at τ_1, τ_2, τ_3, and τ_4 are known. Hence, a starting equation such as the modified Euler or Runge-Kutta technique must be employed. Using the modified Euler technique and the predictor-corrector method, the system of differential equations, Eq. (7), was solved iteratively. Since this problem is boundary valued, it was necessary to make an initial guess of the intensity field at the top ($\tau=\tau_o$) and bottom ($\tau=0$) interfaces before a starting equation could be employed. The initial guess was made by use of a generalized version of the dual beam approximation discussed in Ref. 8. This generalized dual beam approximation (Ref. 14) not only allows guessing the intensity field at $\tau=0$ and $\tau=\tau_o$ but also permits guesses at any of the N stations associated with τ in each of the p quadrature directions corresponding to μ. The quadrature directions of the intensity traveling upward toward the vacuum-deposit interface are μ_ℓ, $\ell=1,\ldots,p/2$, and those associated with intensity traveling toward the deposit-substrate interface are μ_ℓ, $\ell=p/2+1,\ldots,p$.

The actual iteration routine used was a forward and backward integration scheme which proceeds as follows: (1) The input parameters such as refractive indices, optical thickness, and albedo are chosen; (2) the interval between 0 and τ_o is divided into equal intervals at N stations, and the order, p, of the single Gaussian quadrature is selected; (3) the generalized dual beam approximation was used to obtain an initial

guess of the dimensionless radiation field in the p quadrature directions at every τ station. For example, $\tau=\tau_o$, an initial guess was obtained for $i(\tau_o,\mu_\ell)$, $\ell=p/2+1,\ldots,p/2$; (4) Eq. (7), $\ell=p/2+1,\ldots,p$, was integrated backward (downward) over τ from $\tau=\tau_o$ to $\tau=0$ by holding the guessed values of $i(\tau,\mu_\ell)$, $\ell=1,\ldots,p/2$ constant and calculating new values of $i(\tau,\mu_\ell)$, $\ell=p/2+1,\ldots,p$ by use of Eqs. (29) and (30); (5) after arriving at $\tau=0$, the boundary condition, Eq. (9), was used to compute new values of $i(0,\mu_\ell)$, $\ell=1,\ldots,p/2$; (6) Eq. (7), $\ell=1,\ldots,p/2$, was integrated forward (upward) from $\tau=0$ to $\tau=\tau_o$ by holding the newly calculated $i(\tau,\mu_\ell)$, $\ell=p/2+1,\ldots,p$ values constant and computing new values of $i(\tau,\mu_\ell)$, $\ell=1,\ldots,p/2$ through the use of Eqs. (27) and (28) (After arriving at $\tau=\tau_o$ new values of $i(\tau_o,\mu_\ell)$, $\ell=1,\ldots,p/2$ were available.); (7) the values of $\left|i(\tau_o,\mu_\ell)_1 - i(\tau_o,\mu_\ell)_o\right|_\ell$, $\ell=1,\ldots,p/2$ were compared with a given tolerance. (In this case the maximum value had to be less than 0.001. If the difference in any quadrature direction was greater than the given tolerance, the boundary condition, Eq. (8), was used to find new values for $i(\tau_o,\mu_\ell)$, $\ell=p/2+1,\ldots,p$, and the entire backward and forward marching process was begun again at step 4.); (8) the procedure in steps 4 through 7 was continuously repeated until the maximum difference between the values of $i(\tau_o,\mu_\ell)$, $\ell=1,\ldots,p/2$, for two successive iterations was within the given tolerance.

3.4 DEFINITION OF $\rho_{hd}(\mu^1)$

Before proceeding into a discussion of the results, it is necessary to define the hemispherical-directional reflectance. The hemispherical-directional reflectance is the ratio of the intensity reflected from an infinitesimal area, dA, collected in a specific angular direction to the diffusely incident intensity which is hemispherically distributed. Mathematically, the hemispherical-directional reflectance for the problem defined in Fig. 1 is

$$\rho_{hd}(\mu^1) = \rho_{12}(\mu^1) + \frac{i(\tau_o,\mu)}{n_2^2}\left[1-\rho_{21}(\mu)\right] \tag{31}$$

where $(1-1/n_2^2)^{1/2} < \mu \le 1$ and μ is related to μ^1 by Eq. (5). Equation (31) can be used directly in conjunction with Eq. (26) to determine $\rho_{hd}(\mu^1)$ through the source function formulation. For the Chandrasekhar technique and the predictor-corrector method, solution to the transport equation was obtained in terms of the dimensionless intensity in the μ_ℓ quadrature directions. The hemispherical-directional reflectance in terms of the quadrature directions becomes

$$\rho_{hd}(\mu_\ell^1) = \rho_{12}(\mu_\ell^1) + \left[1-\rho_{21}(\mu_\ell)\right]\frac{i(\tau_o,\mu_\ell)}{n_2^2} \tag{32}$$

where $(1-1/n_2^2)^{1/2} < \mu_\ell \leq 1$, $\ell = 1, \ldots, p/2$ with μ_ℓ^1 related to μ_ℓ by Snell's law, Eq. (5). The value of $i(\tau_o, \mu_\ell)$ in Eq. (32) was obtained either from the predictor-corrector solution or from the Chandrasekhar solution via Eq. (15) for $W \neq 1.0$ or via Eq. (16) for $W = 1.0$.

4.0 RESULTS

The results obtained from the three solution techniques will now be compared. Because the numerical agreement of some of the results was so good, it was decided that the results should be illustrated through the use of tables instead of by showing several coincident curves on a figure. Tables 1 and 2 show a comparison of the hemispherical-directional reflectance results predicted by the various methods for $n_2 = 1.2$ and $\tau_o = 0.5$ and 5.0 and corresponding to the various μ_ℓ^1 quadrature directions. The results shown were obtained using a 10-point single Gaussian quadrature. Only $\rho_{hd}(\mu^1)$ in three of the five upward directions is shown since the other two directions correspond to intensity trapped in the coating because of being incident at the coating-vacuum interface at angles greater than the critical angle. Also shown in Tables 1 and 2 are the results obtained by the method of Danilevsky (Ref. 5). This method should be considered as a "library" program since the actual programming of the Danilevsky technique was not performed by the authors of this report.

Table 1. Comparison of $\rho_{hd}(\mu^1)$ Results for the Three Solution Techniques: $n_2 = 1.2$, $W = 0.4$

Substrate	μ_ℓ^1	τ_o	Chandrasekhar	Danilevsky	Numerical Solution	Source Function
Black Paint	0.96220	0.5	0.04557	0.04557	0.04657	0.04774
	0.79850		0.04998	0.04998	0.05008	0.04895
$\bar{n}_3 = 1.48 - i0.00$	0.47403		0.08522	0.08522	0.08795	0.07732
	0.96220	5.0	0.06271	0.06277	0.06271	0.07019
	0.79850		0.06741	0.06741	0.06741	0.07161
	0.47403		0.10120	0.10120	0.10130	0.09893
Steel	0.96220	0.5	0.2527	0.2528	0.2520	0.2567
	0.79850		0.2352	0.2353	0.2363	0.2348
$\bar{n}_3 = 2.48 - i3.43$	0.47403		0.2202	0.2202	0.2272	0.2107
	0.96220	5.0	0.06275	0.06275	0.06271	0.07022
	0.79850		0.06743	0.06743	0.06741	0.07162
	0.47403		0.10120	0.10120	0.10130	0.09895

Table 1. Concluded.

Substrate	μ_ℓ^1	τ_o	Chandrasekhar	Danilevsky	Numerical Solution	Source Function
Aluminum	0.96220	0.5	0.3663	0.3662	0.3676	0.3721
	0.79850		0.3374	0.3374	0.3373	0.3380
$\bar{n}_3$ = 1.44 - i5.32	0.47403		0.2965	0.2965	0.2974	0.2865
	0.96220	5.0	0.06277	0.06271	0.06271	0.07024
	0.79850		0.06744	0.06744	0.06741	0.07164
	0.47403		0.10130	0.10130	0.10130	0.09896
Copper	0.96220	0.5	0.4400	0.4397	0.4418	0.4475
	0.79850		0.4045	0.4044	0.4044	0.4063
$\bar{n}_3$ = 0.82 - i13.00	0.47403		0.3491	0.3490	0.3498	0.3394
	0.96220	5.0	0.06278	0.06278	0.06271	0.07025
	0.79850		0.06744	0.06744	0.06741	0.07165
	0.47403		0.10130	0.10130	0.10130	0.09897

Table 2. Comparison of $\rho_{hd}(\mu^1)$ Results for the Three Solution Techniques: n_2 = 1.2, W = 1.0

Substrate	μ_ℓ^1	τ_o	Chandrasekhar	Danilevsky	Numerical Solution	Source Function
Black Paint	0.96220	0.5	0.1591	0.1591	0.1591	0.1688
	0.79850		0.1742	0.1742	0.1742	0.1698
$\bar{n}_3$ = 1.48 - i0.00	0.47403		0.2293	0.2294	0.2294	0.1951
	0.96220	5.0	0.6903	0.6903	0.6861	NC[a]
	0.79850		0.7058	0.7058	0.7018	
	0.47403		0.7391	0.7391	0.7356	
Steel	0.96220	0.5	0.5011	0.5013	0.5015	0.5338
	0.79850		0.5025	0.5026	0.5029	0.5114
$\bar{n}_3$ = 2.48 - i3.43	0.47403		0.5188	0.5190	0.5192	0.4795
	0.96220	5.0	0.7454	0.7455	0.7407	NC[a]
	0.79850		0.7581	0.7581	0.7535	
	0.47403		0.7854	0.7855	0.7826	
Aluminum	0.96220	0.5	0.7468	0.7468	0.7472	0.7881
	0.79850		0.7444	0.7444	0.7448	0.7626
$\bar{n}_3$ = 1.44 - i5.32	0.47403		0.7453	0.7453	0.7457	0.7243
	0.96220	5.0	0.8222	0.8222	0.8346	NC[a]
	0.79850		0.8310	0.8310	0.8428	
	0.47403		0.8501	0.8501	0.8606	
Copper	0.96220	0.5	0.9615	0.9609	0.9619	0.9951
	0.79850		0.9606	0.9603	0.9611	0.9727
$\bar{n}_3$ = 0.82 - i13.00	0.47403		0.9596	0.9593	0.9601	0.9460
	0.96220	5.0	0.9600	0.9597	0.9709	NC[a]
	0.79850		0.9620	0.9617	0.9723	
	0.47403		0.9663	0.9660	0.9754	

[a] No convergence after 50 iterations using 50, 100, and 200 integration steps for τ_o and 10 quadrature points for the integration with respect to μ in the interval $0 \leq \mu \leq 1$, Eq. (24).

The Danilevsky method was used to compute the coefficients of the characteristic polynominal from the coefficient matrix, Eq. (10). The eigenvalues are the roots of the characteristic polynominal and were determined by the Newton-Raphson method; then the eigenvectors were constructed. With the eigenvalues and eigenvectors known, the integration constants were determined via the Cholesky method. The Danilevsky method, as used here, was found not to be capable of handling a coefficient matrix larger than 16 x 16 since the trace of Eq. (10) yielded a contradiction. The trace, which is the sum of the roots (eigenvalues) of the characteristic polynominal, was no longer equal to the sum of the diagonal elements of the coefficient matrix, Eq. (10). The results obtained by the Danilevsky method have also been included in Tables 1 and 2 as an additional indication of the accuracy of the other results shown.

Table 1 corresponds to W = 0.4, and Table 2 corresponds to results obtained for W = 1.0. The agreement of the results predicted by the various techniques, as illustrated in Table 1, is seen to be good; the agreement obtained by the Chandrasekhar solution, Danilevsky method, and numerical method is excellent. Table 2 (W = 1.0) also shows excellent agreement among the Chandrasekhar solution, Danilevsky method, and numerical solution; however, the successive approximations solution to the integral equation did not converge for large τ_o values. Table 2 also shows poor agreement for the integral equation solution at small τ_o values.

The Chandrasekhar and Danilevsky methods, as expected, were found to be several orders of magnitude faster than the predictor-corrector method or integral equation solution. The Chandrasekhar and Danilevsky methods have the same common disadvantage in that both are applicable only when W is not a function of τ. The Chandrasekhar method is the superior of the two because it permits easier and more accurate determination of the eigenvalues, it is faster with respect to computer time, and (as will be shown) it permits much higher order quadrature approximations (96 x 96) with essentially no sacrifice of accuracy. The Chandrasekhar solution (Eq. 15 or 16) also has the eigenvectors explicitly known, whereas for the Danilevsky method the eigenvectors must be repeatedly constructed. The computation of the eigenvalues by the Chandrasekhar method is extremely fast, and the $\rho_{hd}(\mu^1)$ is directly given by Eqs. (15) or (16) and (32).

For W = 0.4, both the predictor-corrector method and the successive approximations technique (for the integral equation) were found to

converge very rapidly; the amount of computer time required to obtain a solution was about the same for both cases, with the predictor-corrector solution being slightly faster. The predictor-corrector method was probably faster because the dual beam approximation (Ref. 14) was employed as an initial guess criterion. For all practical purposes, however, the two methods are equivalent with respect to computer time. The successive approximations procedure required about 6 iterations to converge, whereas the numerical solution required less than 6 and often only 3 iterations. The predictor-corrector solution was found to have better agreement with the Chandrasekhar results.

For W = 1.0, the Chandrasekhar and Danilevsky methods were again very fast. However, the predictor-corrector technique was found now to require about 12 iterations before converging. This was probably because the initial guess method did not yield as good an initial guess at W = 1.0 as at W = 0.4. In spite of the increased number of iterations, the predictor-corrector solution was still found to be sufficiently fast that its use and accuracy (as seen from Tables 1 and 2) are practical. For W = 1.0, the successive approximations solution for the source function was found to become very slow, with convergence not always attainable even after 50 iterations for τ_o = 5.0, and the accuracy was not good when convergence was attained for τ_o = 0.5. In general it was found that the successive approximations solution of the integral equation became very slow as W → 1.0, and fine $\Delta\tau$ grid (as compared to the predictor-corrector method) was required to achieve good accuracy. Results for W ≤ 0.7 by this method were found to converge in a reasonable amount of computer time. The amount of computer time required for convergence by both the predictor-corrector and successive approximations methods was found to increase as W increased and as τ_o increased. The convergence speed should be expected to decrease as τ_o increases, since the $\Delta\tau_o$ intervals are larger. For very large $\tau_o(\tau_o>7)$ values it is necessary to use more integration steps than the 50 used in the predictor-corrector method. The Chandrasekhar method, on the other hand, can be shown to be applicable even for a semi-infinite medium ($\tau_o \rightarrow \infty$). For the semi-infinite medium, p/2 (or half) of the integration constants in Eq. (15) and (16) become zero.

Now the Chandrasekhar technique will be utilized to compare the results obtained by using either the single or double Gaussian quadrature and also to compare the agreement obtained by using different orders of each type of quadrature. Table 3 shows the angular variation of $\rho_{hd}(\mu^1)$ for τ_o = 0.25 and n_2 = 1.2 and for a range of W for different substrates. The results shown in Table 3 were obtained by using

Table 3. Comparison of $\rho_{hd}(\mu^1)$ Results for the Single and Double Gaussian Quadratures for Various Orders of Quadrature: $n_2 = 1.2$, $\tau_o = 0.25$

Quadrature Type[a]	Quadrature Order	θ_1	Aluminum W = 0.4	Steel W = 0.7	Black Paint W = 1.0
S	96	1.714	0.5442	0.4127	0.0857
S	80	2.054	0.5441	0.4130	0.0859
S	48	3.410	0.5445	0.4132	0.0862
S	96	3.934	0.5442	0.4127	0.0857
S	80	4.716	0.5443	0.4128	0.0858
D	48	4.773	0.5436	0.4118	0.0852
S	32	5.089	0.5448	0.4137	0.0868
D	40	5.704	0.5424	0.4102	0.0840
S	96	6.169	0.5438	0.4125	0.0859
S	24	6.753	0.5401	0.4071	0.0814
D	32	7.087	0.5404	0.4076	0.0819
S	80	7.397	0.5435	0.4124	0.0861
S	48	7.833	0.5436	0.4128	0.0865
S	20	8.073	0.5419	0.4102	0.0844
S	96	8.411	0.5430	0.4122	0.0862
S	16	10.04	0.5442	0.4145	0.0887
S	80	10.09	0.5426	0.4121	0.0865
S	96	10.66	0.5422	0.4118	0.0864
D	48	10.96	0.5415	0.4109	0.0858
D	20	11.14	0.5448	0.4172	0.0910
S	32	11.70	0.5425	0.4127	0.0875
S	48	12.30	0.5418	0.4120	0.0871
S	80	12.79	0.5412	0.4115	0.0868
S	96	12.91	0.5411	0.4114	0.0868
D	40	13.11	0.5424	0.4089	0.0848
S	10	13.12	0.5393	0.4105	0.0873
S	96	15.17	0.5398	0.4108	0.0872
S	80	15.49	0.5396	0.4108	0.0874
S	24	15.55	0.5359	0.4051	0.0826
D	32	16.29	0.5357	0.4054	0.0832
S	48	16.79	0.5390	0.4108	0.0880
D	48	17.21	0.5378	0.4093	0.0870
S	96	17.43	0.5382	0.4101	0.0877
S	80	18.21	0.5377	0.4099	0.0880
S	32	18.41	0.5382	0.4108	0.0889
S	20	18.61	0.5359	0.4075	0.0863
S	96	19.71	0.5364	0.4093	0.0883
D	40	20.58	0.5340	0.4065	0.0865
S	80	20.95	0.5354	0.4089	0.0888
D	10	21.30	0.5263	0.3954	0.0780
S	48	21.32	0.5353	0.4092	0.0893
S	96	22.00	0.5343	0.4084	0.0890
S	16	23.21	0.5349	0.4105	0.0918
D	48	23.49	0.5322	0.4068	0.0889
S	80	23.70	0.5327	0.4077	0.0897

Table 3. Continued

Quadrature Type[a]	Quadrature Order	θ_1	Aluminum W = 0.4	Steel W = 0.7	Black Paint W = 1.0
S	96	24.30	0.5320	0.4074	0.0898
S	24	24.52	0.5280	0.4016	0.0850
S	32	25.21	0.5317	0.4080	0.0911
D	32	25.62	0.5271	0.4016	0.0859
D	20	25.68	0.5344	0.4124	0.0950
S	48	25.90	0.5306	0.4071	0.0909
S	80	26.47	0.5296	0.4064	0.0908
S	96	26.61	0.5294	0.4062	0.0907
D	40	28.13	0.5259	0.4029	0.0893
S	96	28.94	0.5294	0.4050	0.0917
S	80	29.26	0.5262	0.4049	0.0920
S	20	29.45	0.5244	0.4025	0.0902
D	48	29.84	0.5247	0.4036	0.0915
S	10	30.11	0.5145	0.3999	0.0966
S	48	30.55	0.5248	0.4046	0.0931
S	96	31.29	0.5234	0.4037	0.0930
S	80	32.09	0.5223	0.4033	0.0935
S	32	32.15	0.5229	0.4043	0.0944
S	96	33.67	0.5199	0.4022	0.0944
S	24	33.74	0.5159	0.3962	0.0893
S	80	34.95	0.5181	0.4015	0.0953
D	32	35.10	0.5141	0.3959	0.0907
S	48	35.28	0.5178	0.4017	0.0959
D	40	35.80	0.5148	0.3982	0.0936
S	96	36.07	0.5162	0.4007	0.0959
D	48	36.27	0.5152	0.3996	0.0954
S	16	36.94	0.5166	0.4029	0.0994
S	80	37.84	0.5133	0.3996	0.0974
S	96	38.49	0.5121	0.3990	0.0978
S	32	39.30	0.5115	0.3996	0.0996
S	48	40.12	0.5096	0.3985	0.0997
D	20	40.67	0.5125	0.4037	0.1049
S	20	40.75	0.5065	0.3951	0.0978
S	80	40.79	0.5081	0.3976	0.0999
S	96	40.96	0.5077	0.3973	0.1000
D	48	42.83	0.5035	0.3950	0.1011
S	24	43.38	0.4990	0.3893	0.0970
S	96	43.46	0.5031	0.3955	0.1026
D	40	43.65	0.5008	0.3926	0.1004
S	80	43.79	0.5025	0.3954	0.1030
D	32	44.87	0.4965	0.3888	0.0992
S	48	45.12	0.5002	0.3949	0.1050
S	96	46.01	0.4980	0.3937	0.1056
S	32	46.78	0.4973	0.3944	0.1077
S	80	46.87	0.4964	0.3933	0.1068

Table 3. Concluded

Quadrature Type[a]	Quadrature Order	θ_1	Aluminum W = 0.4	Steel W = 0.7	Black Paint W = 1.0
S	10	47.20	→ 0.4679	0.3890	→ 0.1430
S	96	48.62	0.4928	0.3920	0.1093
D	48	49.62	0.4900	0.3903	0.1100
S	80	50.03	0.4899	0.3912	0.1116
D	10	50.07	0.4797	0.3756	→ 0.0986
S	48	50.33	0.4896	0.3915	0.1126
S	96	51.30	0.4872	0.3903	0.1138
D	40	51.84	0.4841	0.3871	0.1123
S	16	51.85	0.4881	0.3932	0.1177
S	20	53.00	0.4819	0.3869	0.1149
S	80	53.30	0.4832	0.3894	0.1178
S	24	53.80	0.4776	0.3823	0.1129
S	96	54.07	0.4815	0.3890	0.1194
S	32	54.82	0.4809	0.3900	0.1223
D	32	55.23	0.4751	0.3824	0.1167
S	48	55.86	0.4784	0.3890	0.1243
S	80	56.72	0.4832	0.3883	0.1261
D	48	56.78	0.4754	0.3871	0.1253
D	20	56.81	0.4808	0.3950	0.1321
S	96	56.94	0.4759	0.3882	0.1266
S	96	59.95	0.4706	0.3884	0.1362
S	80	60.34	0.4701	0.3886	0.1378
D	40	60.71	0.4673	0.3855	0.1364
S	48	61.91	0.4682	0.3899	0.1445
S	96	63.15	0.4663	0.3903	0.1496
S	32	63.92	0.4664	0.3925	0.1548
S	80	64.24	0.4653	0.3917	0.1552
D	48	64.71	0.4641	0.3911	0.1567
S	24	66.05	0.4595	0.3873	0.1593
S	96	66.62	0.4642	0.3957	0.1694
D	32	67.11	0.4598	0.3903	0.1670
S	20	67.82	0.4625	0.3959	0.1756
S	80	68.57	0.4649	0.4010	0.1840
S	48	68.91	0.4656	0.4027	0.1874
S	96	70.48	0.4674	0.4082	0.2013
S	16	70.67	0.4699	0.4123	0.2063
D	40	71.31	0.4670	0.4089	0.2073
S	80	73.68	0.4774	0.4270	0.2401
D	48	74.57	0.4811	0.4329	0.2526
S	96	75.06	0.4847	0.4383	0.2615
S	32	76.14	0.4930	0.4505	0.2820
S	48	78.49	0.5154	0.4808	0.3335
D	20	79.19	0.5283	0.4981	0.3568
S	80	80.78	0.5489	0.5231	0.4002
S	96	81.44	0.5617	0.5386	0.4237

[a] S - Single Gaussian Quadrature D - Double Gaussian Quadrature

single Gaussian quadratures of orders 10, 16, 20, 24, 32, 48, 80, and 96, and double Gaussian quadratures of orders, 10, 20, 32, 40, and 48. Table 3 shows no very large or significant differences from one order of quadrature to the other or in the double quadrature. The points which show the biggest variation from the rest of Table 3 are the quadrature directions which transmitted through the coating-vacuum interface into the largest θ_1 directions for p = 10. As noted by the arrows in Table 3, θ_1 = 47.20 and θ_1 = 50.07 show the largest variation, and both correspond to p = 10 for the single and double Gaussian quadratures, respectively. To clarify what is meant by quadrature order in Table 3, a 32-point quadrature (double or single) means 16 positive and 16 negative quadrature directions; or, the quadrature order can be considered as the size of the p x p coefficient matrix in Eq. (10) (in this case, 32 x 32). Figure 3 is a graphical representation of some of the results in Table 3 and is presented in order to more clearly illustrate the agreement between the single and double Gaussian quadratures for n_2 = 1.2. Table 3 and Fig. 3 show that there is essentially no advantage with respect to accuracy in using one type of Gaussian quadrature over the other. However, from a computational point of view, it is recommended since both are essentially the same, that the single Gaussian quadrature

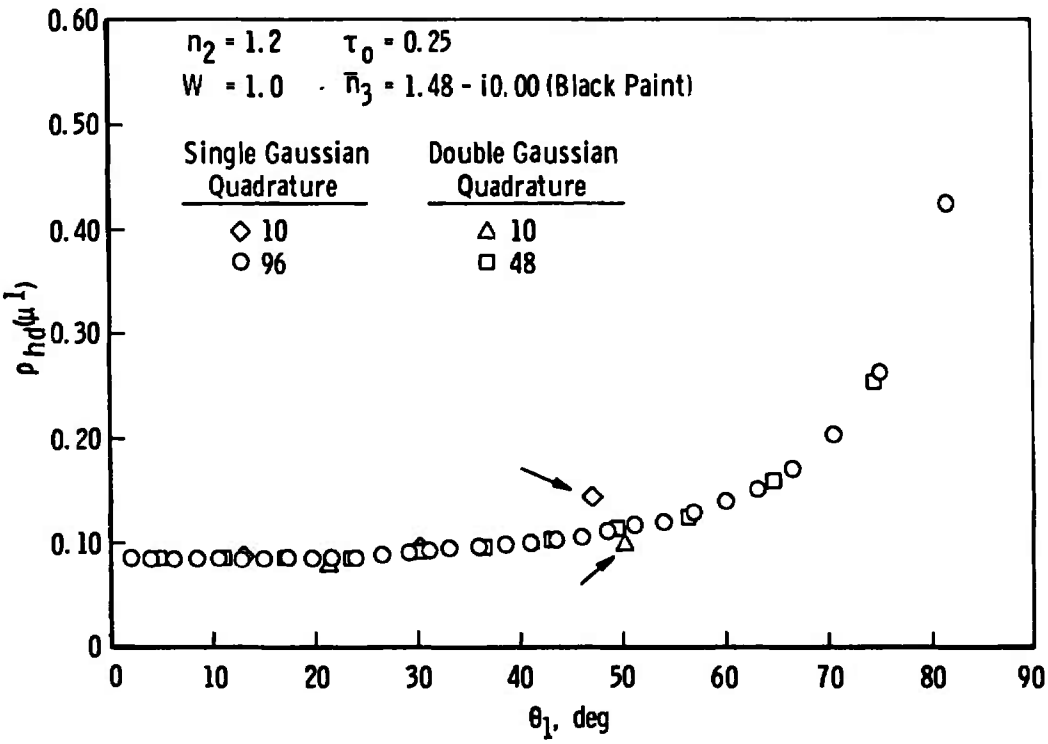

Figure 3. Comparison of $\rho_{hd}(\mu^1)$ results for various orders of single and double Gaussian quadratures.

be used. There are two reasons for this. First, for a given order of quadrature, the largest eigenvalue is much smaller for the single Gaussian quadrature than for the double Gaussian quadrature, as is shown in Fig. 4. (The results shown in Fig. 4 can be considered valid for all values of W since the size of the maximum eigenvalue only changes by about ±1 on the ordinate scale in going from W = 0.0 to W = 1.0.) This means that computations can be made to a much larger optical thickness, τ_0, with the single quadrature than with the double quadrature since this largest eigenvalue occurs as a positive number in the exponent of Eqs. (15) and (16); the double quadrature will cause computer overflow at a much smaller τ_0 value. The second advantage is that the double quadrature directions correspond to larger angles than do the single quadrature directions. This means that more double quadrature

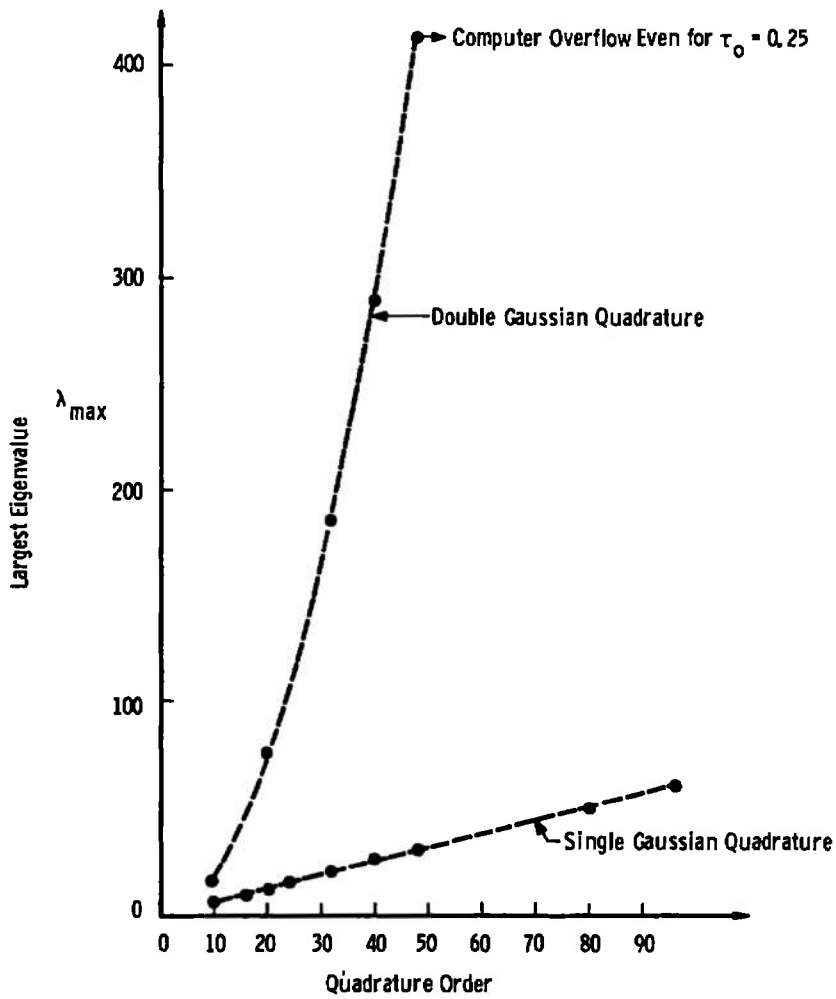

Figure 4. Effect of quadrature order on maximum eigenvalue.

directions are greater than the critical angle, and thus $\rho_{hd}(\mu^1)$ is computed in fewer directions for the double quadrature since the others are trapped inside the coating. This situation becomes even more evident as the refractive index n_2 increases. The advantage of having more quadrature directions transmit through the coating-vacuum interface is that the flux can be more accurately evaluated since the intensity is known in more directions. Figure 5 demonstrates the difference between the number of transmitted directions for the single and double quadratures an n_2 increases.

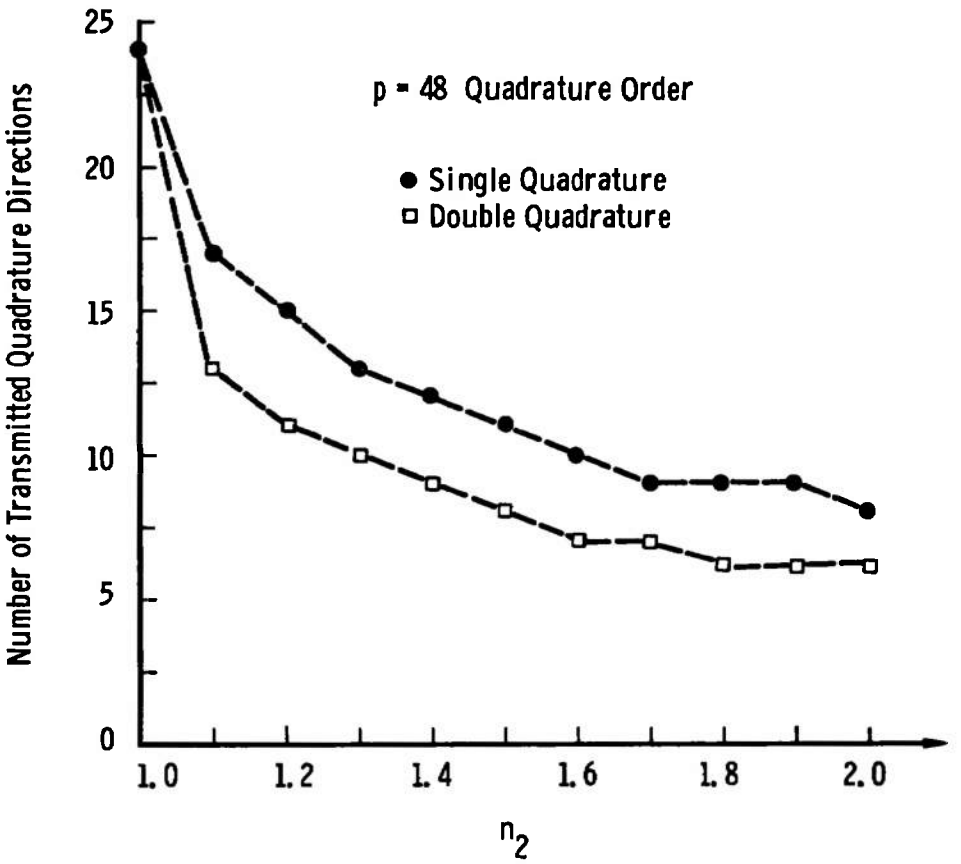

Figure 5. Effect of refractive index on number of transmitted quadrature directions.

Figure 6 shows that for $n_2 = 1.4$ a 16-point single Gaussian quadrature must be used to achieve accuracy. Results are shown for both $\tau_o = 0.25$ and $\tau_o = 5.0$. The 10-point Gaussian quadrature is seen to yield results that are too low. Whereas the 10-point quadrature showed

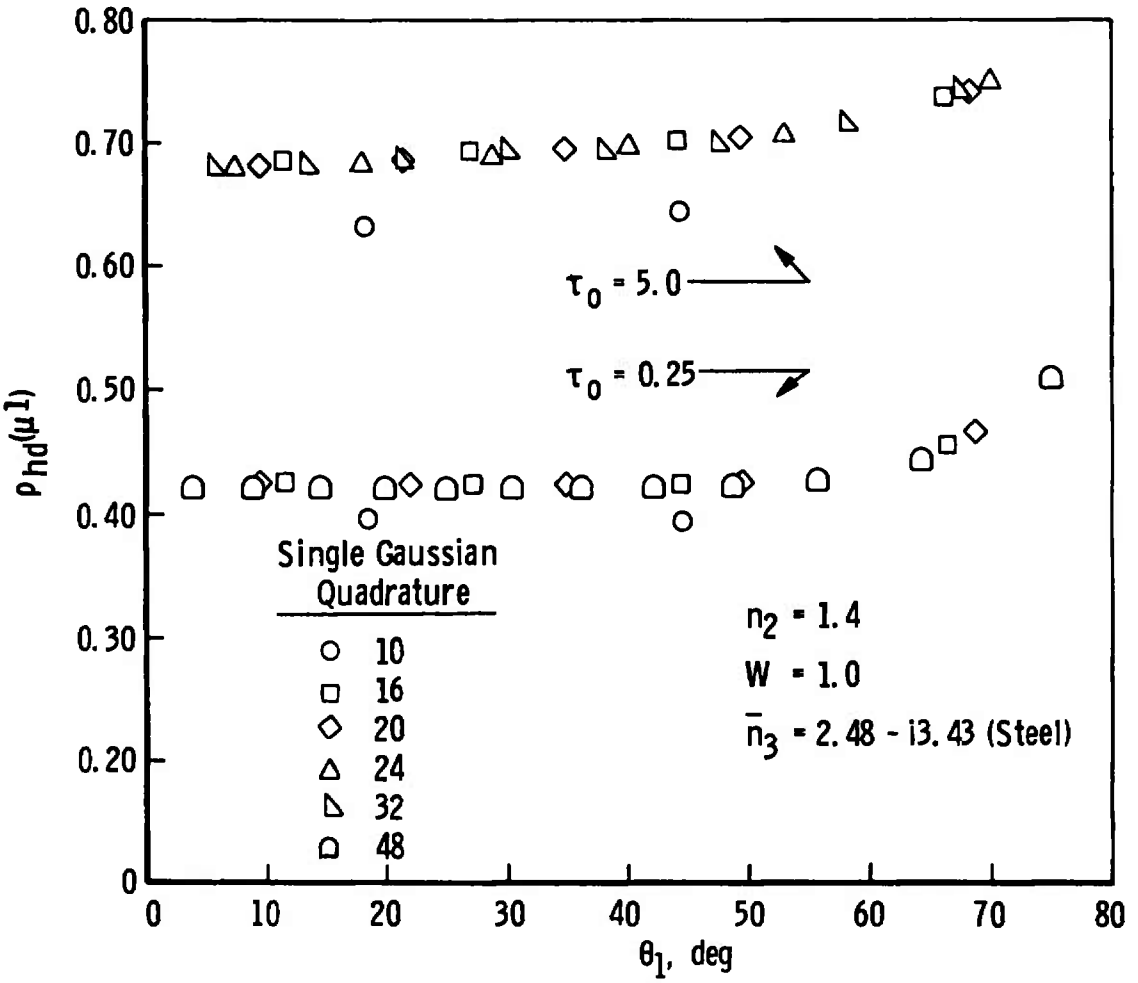

Figure 6. Order of quadrature needed to achieve accuracy for $n_2 = 1.4$.

good agreement in Fig. 3 for $n_2 = 1.2$ (except for large θ_1), it is seen that for $n_2 = 1.4$ a higher order quadrature is needed for accuracy. This gives rise to speculation that as n_2 increases the order of Gaussian quadrature needed for accuracy also increases; Fig. 7 shows this to be true. The results shown in Fig. 7 were obtained by increasing the quadrature order until two successive higher order quadratures showed good agreement. The results given in Fig. 7 should be considered as the minimum quadrature order needed for accuracy. Higher order quadratures than those shown will likewise yield good accuracy. Although Fig. 7 is for the single Gaussian quadrature, results were obtained for the double Gaussian quadrature which also showed the same dependence of accuracy upon quadrature order. Hence, Fig. 7 may be considered valid for both the double and single Gaussian quadratures.

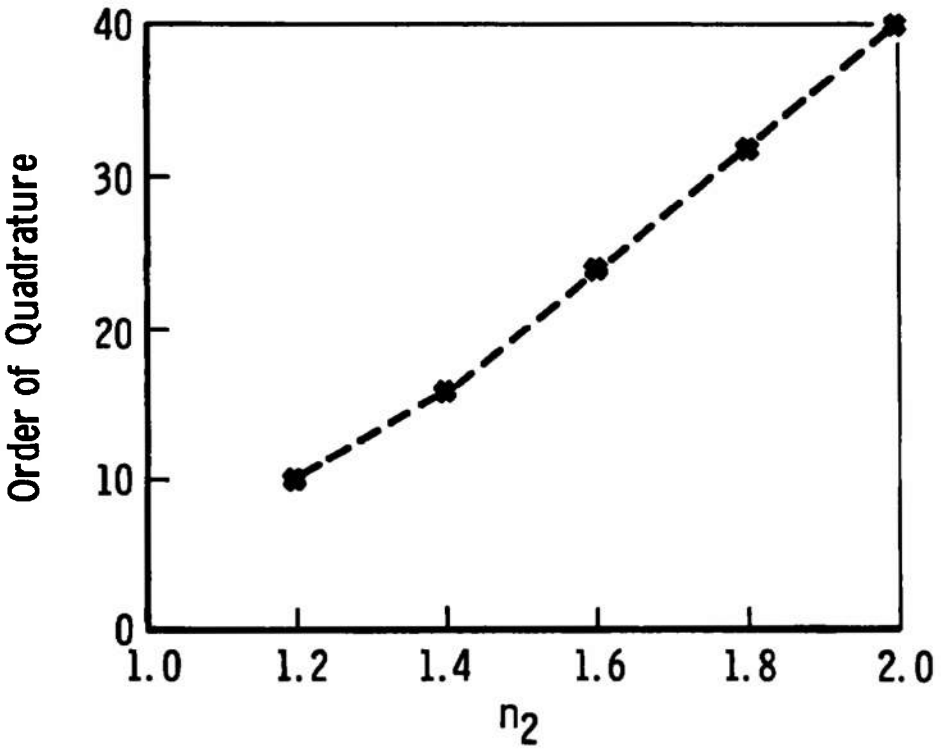

Figure 7. Effect of coating refractive index on quadrature order required for accuracy.

5.0 DISCUSSION OF ERROR

The three solution techniques and numerical formulas used in the solution of the transport equation were described in the analysis section of this report. A discussion of the error is now presented so that confidence in the results presented may be achieved. First, the Chandrasekhar method will be discussed, and then the numerical solution and successive approximations solution will be discussed. From the discussion of the results in Table 3 it is concluded that the error introduced in using one type of quadrature as opposed to the other or different orders of quadrature is negligible. Thus the error discussed here will pertain to using a fixed order of quadrature. For the Chandrasekhar solution, the roots (λ^2) of Eq. (13) were found by an iterative procedure, and the λ^2 values were considered to have been determined when two consecutive calculations were within 10^{-12} (double) precision) of one another. Thus the eigenvalues ($\pm\lambda$) were accurate to 10^{-6}. Once the homogeneous solution, Eq. (15) or (16), was obtained,

it became possible for error to be introduced in the determination of the p integration constants. In order to estimate the error introduced through the Cholesky method, which was used to determine the integration constants, the solutions, Eqs. (15) and (16), were put back into the boundary conditions. The right sides of Eqs. (8) and (9) were subtracted from the left sides for each of the p/2 quadrature directions corresponding to each equation. This was done for both the double and single Gaussian quadratures, for W = 0.4, 0.7, 1.0, for the four substrates used in Table 1, and for τ_0 = 0.25. It was found that the largest difference between the two sides of Eqs. (8) and (9) occurs at the small optical thicknesses. Thus, Fig. 8 is shown for the small optical thickness, τ_0 = 0.25.

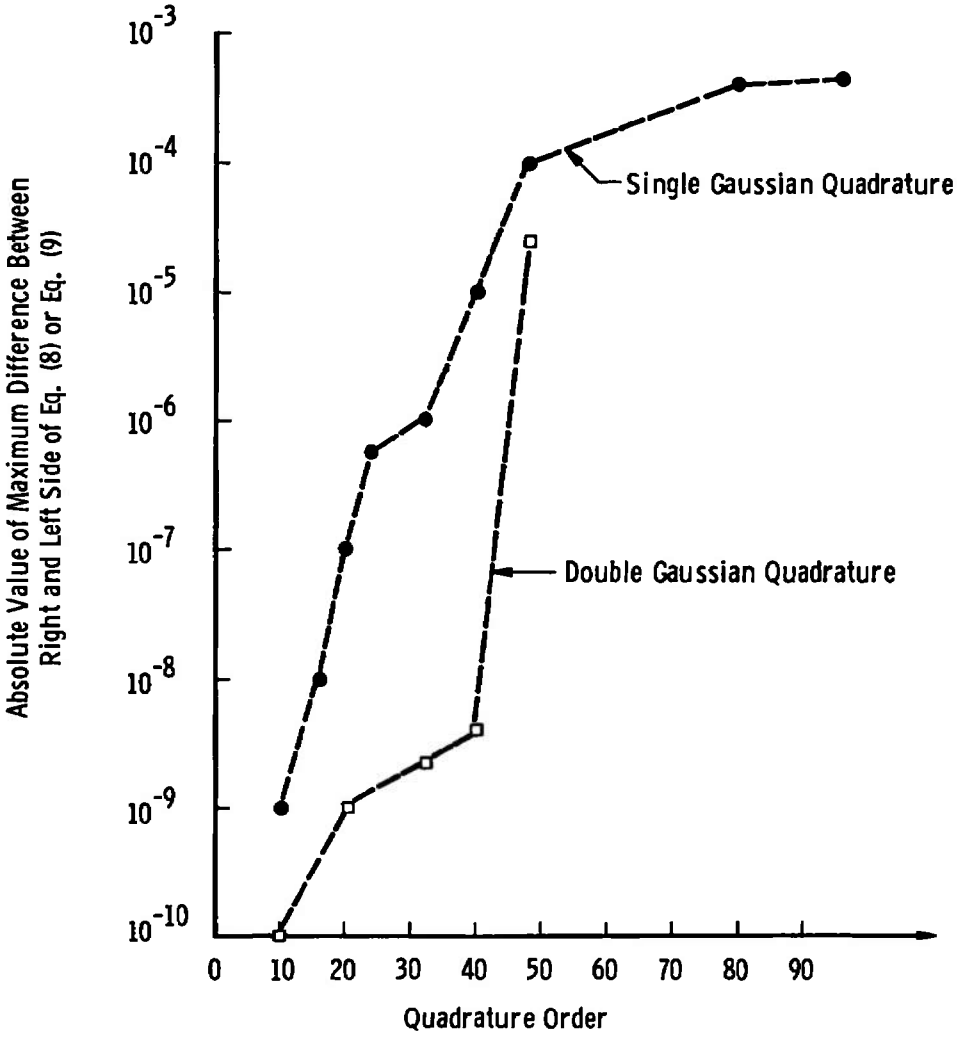

Figure 8. Effect of quadrature order on maximum error for Chandrasekhar method, τ_0 = 0.25.

Figure 8 shows the maximum error of all the quadrature directions as a function of quadrature order; again, this error represents the maximum difference between the right and left sides of Eqs. (8) and (9) for the range of conditions described above. It is seen here that the double quadrature yields better accuracy than the single quadrature; however, Fig. 8 shows the error for both types and all orders of quadrature to be negligible. The conclusion is that use of the Cholesky method introduced very little error into the final solution.

Regarding the numerical solution, it should be remembered that all numerical formulas are approximate since they usually involve the truncation of a Taylor series. The evaluation of error associated with the numerical solution is also approximate. The purpose of the error term is to offer a means of obtaining a general idea of the error committed by numerical solution using a particular step size.

The predictor-corrector method is very convenient because it provides a simple expression for the error per step estimate. Call $E_{pr}(\tau_{n+1})$ the error in computing $i_{pr}(\tau_{n+1})$ by using Eq. (27); call $E_{co}(\tau_{n+1})$ the error in computing $i_{co}(\tau_{n+1})$ by using Eq. (25) to correct this predicted value of $i_{pr}(\tau_{n+1})$. Let $Y(\tau_{n-1})$ be the actual value of $i(\tau_{n+1})$; then

$$E_{co}(\tau_{n+1}) = Y(\tau_{n+1}) - i_{co}(\tau_{n+1}) \tag{33}$$

$$E_{pr}(\tau_{n+1}) = Y(\tau_{n+1}) \; i_{pr}(\tau_{n+1}) \tag{34}$$

Subtracting the first equation from the second gives

$$i_{co}(\tau_{n+1}) - i_{pr}(\tau_{n+1}) = E_{pr}(\tau_{n+1}) - E_{co}(\tau_{n+1}) \tag{35}$$

The expressions for the error terms of the predictor and corrector are given respectively by

$$E_{pr}(\tau_{n+1}) = \frac{28}{90} h^5 \, i^{(5)}(X_1) \tag{36}$$

and

$$E_{co}(\tau_{n+1}) = -\frac{1}{90} h^5 \, i^{(5)}(X_2) \tag{37}$$

where X_1 is contained in the interval (τ_{n-3}, τ_{n+1}) and X_2 is contained in the interval (τ_{n-1}, τ_{n+1}). Let the assumption be made that h is sufficiently small that the variation between $i^{(5)}(X_1)$ and $i^{(5)}(X_2)$ is

negligible; then a small error is committed by using $i^{(5)}(X)$ as their approximate common value. Hence subtracting Eq. (37) from Eq. (36) and replacing $i^{(5)}(X_1)$ and $i^{(5)}(X_2)$ with $i^{(5)}(\bar{X})$ results in

$$E_{pr}(\tau_{n+1}) - E_{co}(\tau_{n+1}) = \frac{29}{90} h^5 i^{(5)}(X) \tag{38}$$

Combining Eqs. (35) and (38) yields

$$i_{co}(\tau_{n-1}) - i_{pr}(\tau_{n+1}) = \frac{29}{90} h^5 i^{(5)}(X) \simeq -29E_{co}(\tau_{n+1}) \tag{39}$$

and therefore,

$$E_{co}(\tau_{n-1}) = [i_{pr}(\tau_{n-1}) - i_{co}(\tau_{n+1})]/29 \tag{40}$$

Equation (40) gives an approximate formula for the error commited per step of numerical integration by the Milne predictor-corrector method.

For the purpose of plotting results which would indicate the significant general trends, it was decided that the total maximum error between two successive iterations of $i(\tau_o, \mu)$ $[i = 1, \ldots, p/2]$ should be less than 0.001; thus the error per step should be less than 0.001 divided by the total number of steps. Since 50 steps were used, the difference between predictor and corrector at any station, τ, for each quadrature direction should be

$$i_{pr}(\tau_{n+1}) - i_{co}(\tau_{n+1}) = 29\, E_{co}(\tau_{n+1}) \tag{41}$$

and the value of $E_{co}(\tau_{n+1})$ is approximated by

$$E_{co}(\tau_{n+1}) = \frac{0.001}{\text{No. steps}} = \frac{0.001}{50} = 0.00002 \tag{42}$$

Thus, at each integration station it was required that $i_{pr} - i_{co} < 0.00058$. Since the maximum optical thickness used was $\tau_o = 5.0$, this corresponds to a "maximum" value of h = 0.1. Since by Eq. (37) the error per step is on the order of h^5, the value of $E_{co}(\tau_{n+1}) \simeq 0.00001$, which is less than the value required by Eq. (42). The values presented correspond to the maximum error, and again it should be mentioned that these expressions give only a reasonable estimate of the error committed. If the difference between predictor and corrector is not less than 0.00058, the corrector may be used again and again until two successive calculations are within the given tolerance. It was not necessary to use the

corrector more than once except for $\tau_o = 5.0$, where at a few stations it was necessary for multiple use. For the results requiring a maximum error of 0.001 in $i(\tau_o, \mu_\ell)$ $[\ell = 1, \ldots, p/2]$ between two successive iterations, it was only necessary to perform the calculations in single precision, as will be shown later. By an analysis similar to that just presented it was possible to specify a maximum error of 10^{-5} between two successive iterations of $i(\tau_o, \mu_\ell)$ $[\ell = 1, \ldots, p/2]$, if the calculations were performed in double precision.

So far only the analysis for approximating the error associated with the numerical formula has been presented. There are also round-off errors associated with any numerical calculation scheme. An effective procedure for determining the magnitude of the round-off error is to first carry out a calculation in single precision and then to use double precision to see if any significant difference is present. However, the formula errors and round-off errors are usually coupled together in such a way that they cannot be separately approximated.

Probably the most effective method of approximation of the coupled error is not only to use double and single precision but also to simultaneously reduce the step size to one half its previous value and see if any significant changes occur. In an attempt to make sure that the accuracy of the solution was within the stated tolerance, the numerical solution using the 10-point single Gaussian quadrature was performed in both double and single precision and also for various step sizes. Table 4 illustrates a comparison of the results for various step sizes and for the single and double precision calculations. As should be expected, the results at the small optical thickness are much more accurate than those of the large optical thickness since the corresponding step size is one-tenth that of the larger optical-thickness step size. As shown earlier in Table 1, these results are also in good agreement with the results obtained by the Chandrasekhar solution.

Also shown in Table 4 is the sensitivity of the successive approximations solution to the integration step size. The results shown are for demonstration purposes, and only single precision calculations were performed. As in the predictor-corrector discussion, the error analysis was performed indirectly by varying the integration step size. Hence the solution of the integral equation is seen to be essentially insensitive to the integration step size.

Table 4. $\rho_{hd}(\mu^1)$ Results for Various Step Sizes for the Milne Predictor-Corrector Technique, n_2 = 1.2, W = 1.0, and for the Source Function Method, n_2 = 1.2, W = 0.4

			Predictor-Corrector, W = 1.0					Source Function, W = 0.4	
			Double Precision		Single Precision			Single Precision	
Substrate	μ_1	τ_o	50 Steps	100 Steps	50 Steps	100 Steps	200 Steps	50 Steps	100 Steps
Black Paint	0.96220	0.5	0.1591	0.1591	0.1591	0.1591	0.1591	0.04774	0.04771
	0.79850		0.1742	0.1742	0.1742	0.1742	0.1742	0.04895	0.04892
	0.47403		0.2294	0.2294	0.2294	0.2294	0.2294	0.07732	0.07729
n = 1.48 - i0.00	0.96220	5.0	0.6863	0.6961	0.6878	0.6878	0.6877	0.07019	0.06692
	0.79850		0.7019	0.7018	0.7052	0.7033	0.7032	0.07161	0.06834
	0.47403		0.7356	0.7356	0.7367	0.7368	0.7366	0.09893	0.09576
Steel	0.96220	0.5	0.5015	0.5015	0.5015	0.5015	0.5015	0.2567	0.2567
	0.79850		0.5029	0.5029	0.5029	0.5029	0.5028	0.2348	0.2347
	0.47403		0.5192	0.5192	0.5192	0.5192	0.5192	0.2107	0.2106
n = 2.48 - i3.43	0.96220	5.0	0.7404	0.7407	0.7423	0.7423	0.7422	0.07022	0.06695
	0.79850		0.7533	0.7535	0.7550	0.7550	0.7549	0.07162	0.06836
	0.47403		0.7813	0.7826	0.7826	0.7826	0.7825	0.09895	0.09577
Aluminum	0.96220	0.5	0.7472	0.7472	0.7472	0.7472	0.7471	0.3721	0.3720
	0.79850		0.7448	0.7448	0.7447	0.7447	0.7446	0.3380	0.3379
	0.47403		0.7457	0.7457	0.7457	0.7457	0.7456	0.2865	0.2865
n = 1.44 - i5.32	0.96220	5.0	0.8346	0.8346	0.8346	0.8346	0.8345	0.07024	0.06698
	0.79850		0.8428	0.8428	0.8428	0.8428	0.8427	0.07164	0.06838
	0.47403		0.8606	0.8606	0.8606	0.8606	0.8605	0.09896	0.09579
Copper	0.96220	0.5	0.9619	0.9619	0.9613	0.9613	0.9612	0.4475	0.4474
	0.79850		0.9611	0.9611	0.9607	0.9607	0.9606	0.4063	0.4062
	0.47403		0.9601	0.9601	0.9598	0.9598	0.9597	0.3394	0.3393
n = 0.82 - i13.00	0.96220	5.0	0.9709	0.9709	0.9706	0.9706	0.9705	0.07025	0.06699
	0.79850		0.9723	0.9723	0.9721	0.9720	0.9720	0.07165	0.06839
	0.47403		0.9755	0.9754	0.9752	0.9752	0.9751	0.09897	0.09580

6.0 SUMMARY AND CONCLUSIONS

Three solution techniques to the radiative transport equation have been demonstrated on a sample problem, and a comparison of the three methods has been presented. In addition, a comparison of different orders of Gaussian quadrature was presented for both the double and single Gaussian quadrature approximations. The Chandrasekhar solution was found to be extremely fast; only the computation of the eigenvalues required iteration, and this procedure converged rapidly since the bounds for each eigenvalue were known. The Milne predictor-corrector solution also converged very rapidly and yielded results which agreed extremely well with the Chandrasekhar solution for all four substrates, for all values of W, for all $\tau_o(0 \rightarrow 5.0)$, and for all viewing angles. The successive approximations solution to the integral equation formulation was also found to converge rapidly for small values

of W($W \leq 0.70$). However, for large values of W($0.70 < W \leq 1.0$) the integral equation solution was found to converge very slowly, and even when a solution was obtained, its accuracy was not good. After the three solution techniques were compared, the Chandrasekhar method was used to compare various orders of Gaussian quadratures for both the single and double approximations. Comparison of the double and single approximations for a fixed order of quadrature showed very little difference in accuracy. However, it was found that as the coating refractive index increased, the order of the Gaussian quadrature had to be increased to maintain accuracy. From a computational point of view, the single Gaussian quadrature was seen to have two advantages over the double quadrature. First, the largest eigenvalue is considerably smaller for the single quadrature approximation, thus allowing computation to much larger τ_o values before encountering computer overflow. Second, the double quadrature directions correspond to larger angles measured from the substrate normal. This means that more quadrature directions are trapped inside the coating past the critical angle; the result is that the single quadrature approximation has more quadrature directions which transmit through the coating-vacuum interface. Hence more information is transmitted in more directions. This implies integration with respect to μ^1 in determining that flux can more accurately be performed.

Finally, a discussion of error for each technique was given, and the sensitivity of the predictor-corrector and successive approximations solutions to finite-difference step size was shown. All three methods presented are easy to understand and use; also, the Chandrasekhar method can be used as an initial guess criterion for the other techniques when W is a function of τ. Furthermore, all three techniques can be extended to include emission (particular solutions) and anisotropic scattering.

The results discussed here are important in choosing which technique to use when solving the radiative transport equation. The solution to the transport equation is a powerful tool to be employed in determining the reflectance and transmittance behavior of absorbing and scattering condensed gas coatings as a function of viewing angle, coating thickness, absorption, scattering, and substrate effects. Also, the solution to the transport equation can be used in conjunction with experimental data for determining the coating thickness and optical properties of condensed gases.

REFERENCES

1. Roux, J. A., Smith, A. M., and Shahrokhi, F. "Radiative Transfer Properties of High Albedo CO_2 and H_2O Cryodeposits." AIAA Progress in Astronautics and Aeronautics: Thermal Control and Radiation. Vol. 31, edited by C. L. Tien, MIT Press, Cambridge, Mass., 1973, pp. 369-388.

2. Wolf, P. "An Analytical and Experimental Study of the Radiant Heat Transfer in Scattering, Absorbing, and Emitting Media." Ph. D. dissertation, 1968, University of Tennessee.

3. Merriam, R. L. "A Study of Radiative Characteristics of Condensed Gas Deposits on Cold Surfaces." Ph. D. dissertation, 1968, Purdue University.

4. Hottel, H. C., Sarofim, A. F., Evans, L. B., and Vasalos, I. A. "Radiative Transfer in Anisotropically Scattering Media: Allowance for Fresnel Reflection at the Boundaries." Journal of Heat Transfer, Vol. 90, Series C, No. 1, February, 1968, pp. 56-62.

5. Faddeeva, V. N. Computational Methods of Linear Algebra. Dover Publications, Inc., New York, 1959.

6. Hsia, H. M. and Love, T. J. "Radiative Heat Transfer Between Parallel Plates Separated by a Nonisothermal Medium with Anisotropic Scattering." Journal of Heat Transfer, Vol. 89, Series C, August 1967, pp. 197-203.

7. Chandrasekhar, S. Radiative Transfer. Dover Publications, Inc., New York, 1960.

8. Hottel, H. C. and Sarofim, A. F. Radiative Transfer. McGraw-Hill Book Company, New York, 1967.

9. Callis, L. B. "The Radiative Transfer Equation and Environmental Effects in the Upper Atmosphere." AIAA Paper 72-663, June 1972.

10. Sykes, J. B. "Approximate Integration of the Equation of Transfer." Monthly Notes, Royal Astronomical Society, Vol. 111, 1951.

11. Roux, J. A., Todd, D. C., and Smith, A. M. "Eigenvalues and Eigenvectors for Solutions to the Radiative Transport Equation." AIAA Journal, Vol. 10, No. 7, July 1972, pp. 973-976.

12. Franklin, J. N. Matrix Theory. Prentice-Hall, Inc., Englewood Cliffs, New Jersey, 1968, p. 203.

13. Roux, J. A., Todd, D. C., and Smith, A. M. "Erratum: Eigenvalues and Eigenvectors for Solutions to the Radiative Transport Equation." AIAA Journal, Vol. 11, No. 5, May 1973, pp. 767-768.

14. Roux, J. A. "Radiative Heat Transfer of Coatings on a Cryogenic Surface." Ph. D. dissertation, 1970, University of Tennessee. Also available as AEDC-TR-71-90 (AD722720), April 1971.